Polygons on a rotating thin-water layer: a combined experimental and numerical approach

Sébastien Poncet

POLYGONS ON A ROTATING THIN-WATER LAYER: A COMBINED EXPERIMENTAL AND NUMERICAL APPROACH

S. Poncet

Aix-Marseille University, M2P2 UMR 7340, 38 rue F. Joliot-Curie, 13451 Marseille, France

Abstract

The flow of a thin fluid layer over a rotating disk is studied by direct numerical simulation and flow visualizations. The primary bifurcation appears as spectacular sharp-cornered polygonal patterns located along the outer casing. The stability diagram is established experimentally and confirmed numerically with a strong hysteresis between the spin-up and spin-down phases. These structures are induced by the appearance of a secondary flow. They rotate at a frequency, which slightly increases with the number of vortices. For larger Reynolds numbers, the polygons may coexist with a crossflow instability appearing as positive spirals.

Keywords: rotating flow, free surface, shear-layer instability, DNS, flow visualizations.

1 Introduction

The present work is concerned with the stability of a water layer over a rotating disk, leading to steady modes of a shear-layer instability. Shear layers in rapidly rotating systems are of primary importance in geophysics, as they can be observed in oceans, hurricanes or planetary atmospheres but also in computer hard drives. The stability of a fluid layer over a rotating disk is governed by many parameters whose the aspect ratio of the cavity $G = e/R_o$ (e the water depth at rest and R_o the disk radius). For $G > 0.15$, the polygons appear at high rotation rates such that a dry central zone may occur close to the rotation axis and the Froude number $Fr = \Omega^2 R_o/g$ (Ω the disk rotation rate) pilots the instability mechanisms. The surface flow may be divided into two regions: an inner center in solid body rotation and an outer annulus, where a weak secondary flow occurs [1, 2]. For $G < 0.15$, the transition mechanisms are quite different [3, 4]. The experimental data of Poncet and Chauve [3] are here revisited and underpinned by new simulations in this case.

2 Experimental and numerical methods

The cavity consists of a smooth disk (radius $R_o = 140$) mm rotating at Ω enclosed by a cylindrical shroud (radius $R_o + j$, $j = 0.85$ mm). A central hub (radius R_i) may be attached to the rotor. The cavity is filled up by water (kinematic viscosity $\nu = 10^{-6}$ m^2/s), seeded with reflective particles of kalliroscope. The water depth at rest is denoted e. The flow is mainly controlled by three parameters: the rotational Reynolds number $Re = \Omega R_o^2/\nu$, the aspect ratio $G = e/R_o$ of the cavity and its radius ratio $\eta = R_i/R_o$. Images (768×576 pixels) are taken at a video frequency of 25 Hz. Between two observations, Ω is increased (spin-up) or decreased (spin-down) by step of 1 rpm and one respects the Ekman time scale $\tau_E = \sqrt{Re}/\Omega$ [3].

The numerical approach is based on a pseudospectral technique using a collocation-Chebyshev method in the radial and axial directions and a Galerkin-Fourier method in the azimuthal direction. This approximation is applied at the Gauss-Lobatto collocation points in the radial and axial directions. In the azimuthal direction, a uniform distribution is considered. The time scheme is semi-implicit and second-order accurate. The solution method is based on an efficient projection scheme to solve the velocity-pressure coupling. Finally, for each Fourier mode, a full diagonalization technique is used and yields simple matrix products for the solution of successive two-dimensional uncoupled Helmholtz and Poisson equations at each time step. The free surface is assumed to be flat and undeformable as the Froude number Fr remains small (here max(Fr)$= 0.027 << 1$).

3 Results

Modes $m = 8$ to 3 have been observed for different combinations of Re and G (Fig.1). The influence of the radius ratio η is discussed in detail in [3]. The flow is divided into two regions: the inner region in solid body rotation and the outer region where the vortices occur, separated by a polygonal boundary. Figure 2a presents the marginal stability diagram of the first polygonal mode in the plane (Re, G) for $\eta = 0$ during spin-up. The present experimental and numerical results compare quite well with the stability analysis of Kahouadji [4] for $G \geq 0.07$. When G decreases, Re and m increase. Kahouadji [4] developed also a curvilinear formulation to take into account the deformation of the free surface and tried to explain the discrepancies between the flow visualizations and the stability analysis for $G \leq 0.06$. But it did not improve the present results for a flat free surface. The secondary bifurcations are shown in Figure 2b for $\eta = 0$. Strong hysteresis cycles are observed as illustrated in Figure 2c. The same kind of sequence is observed for all values of G: N polygonal patterns are observed during spin-up and $N-1$ during spin-down. From DNS, the $m = 5$ instability threshold is $Re = 18000$ during spin-up, while this mode remains stable up to $Re = 15000$ during spin-down, highlighting the subcritical nature of this instability.

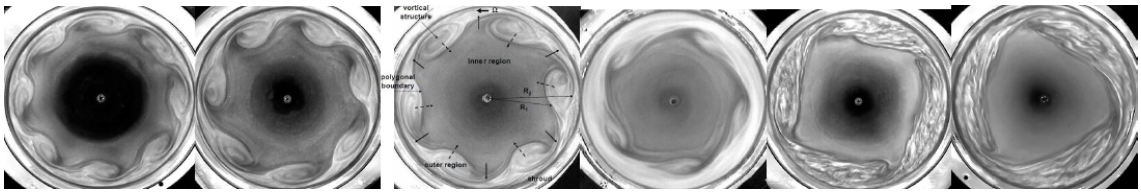

Figure 1: Flow visualizations of the modes $m = 8$ to 3 for $\eta = 0$. The disk rotates counterclockwise.

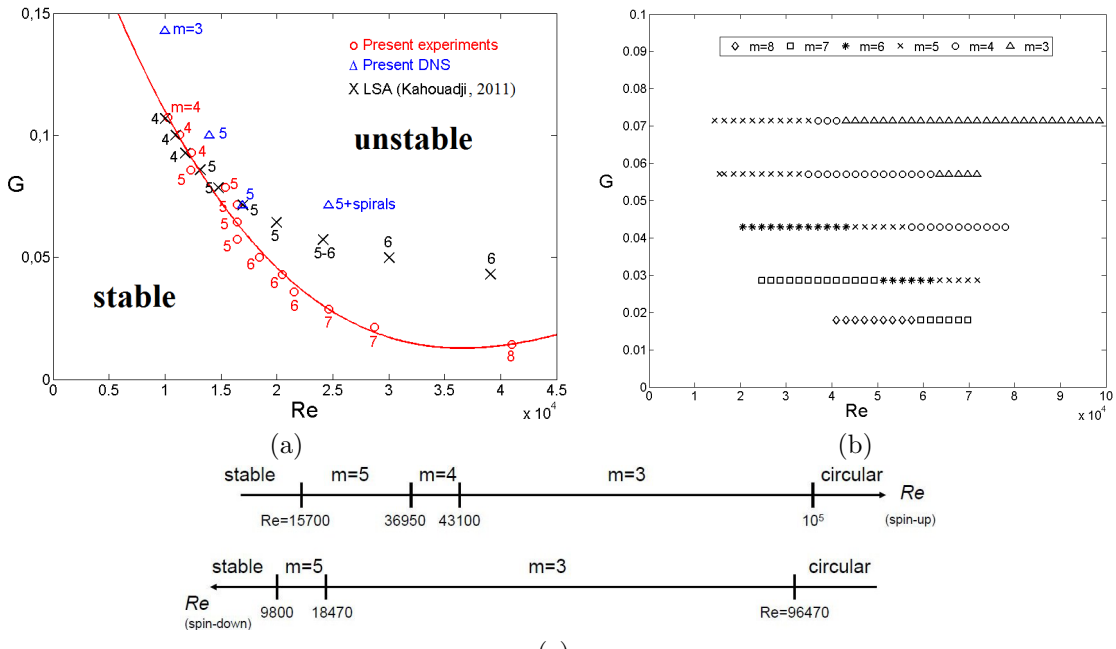

Figure 2: Stability diagrams obtained for $\eta = 0$ during spin-up: (a) in a (Re, G) plane for the primary bifurcation; (b) complete experimental diagram and (c) hysteresis cycle for $G = 0.0714$.

From experiments, the first polygonal mode m (spin-up) can be scaled by: $m \sim -2.26 \times E_e^{-1/4}$ ($E_e = (G^2 Re)^{-1}$ the Ekman number), as also observed by Moisy et *al.* [5] in counter-rotating disk flows. It confirms that the boundary layer along the shroud is a Stewartson layer, whose thickness is $E_e^{-1/4} R_o$. Niino and Misawa [6] proposed a Reynolds number $Re_{NM} = VL/\nu$, as the

only parameter governing the flow stability, where $L = e(E_e/4)^{1/4}$ is the shear layer thickness. In the present case, the critical Reynolds number Re_{NM} is constant: $Re_{NM} \simeq 248$ ($V = \Omega R_o$), to be compared to $Re_{NM} \simeq 11.7$ for [6] and $Re_{NM} \simeq 110$ for [5]. It is noticeable also that the critical radius $r_c = (R_1 + R_2)/2$ for the appearance of the polygons remains constant: $r_c \simeq 0.73 R_o$.

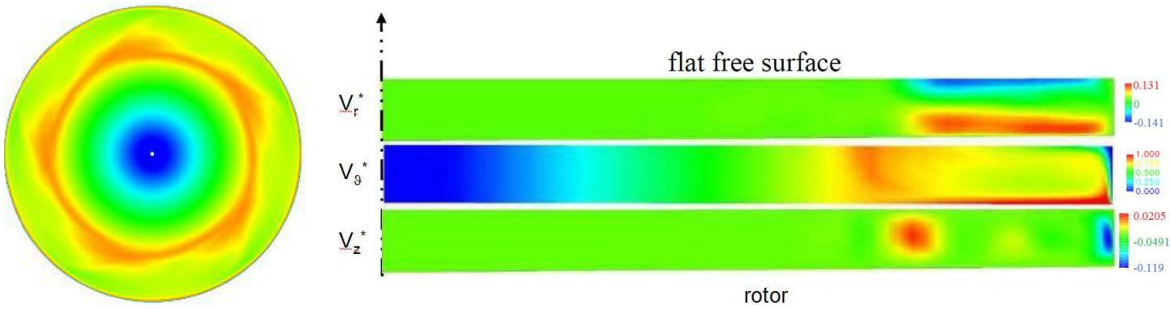

(a) (b)

Figure 3: Maps of (a) the tangential velocity in a (r, θ) plane at $z/e = 0.32$ and of (b) the three velocity components in a ($r \in [0, R_o + j]$, $z \in [0, e]$) plane obtained from DNS for $Re = 18000$, $G = 0.0714$ and $\eta = 0$ ($130 \times 128 \times 65$ mesh points in the (r, θ, z) directions with $\delta t = 10^{-4}\Omega^{-1}$).

Figure 3 present the flow structure of the pentagon. It confirms that the flow is in solid body rotation in an inner region and that a secondary flow developed at the periphery. The fluid moves radially outwards along the rotor and inwards along the free surface. The map of the axial velocity clearly shows this recirculation zone at the origin of the mode $m = 5$. The polygonal structures do not rotate at the same rotation speed as the rotor. One can define the frequency ratio $F = \Omega_f/\Omega$ between the polygon and disk rotation rates. Figure 4 presents its variation with the Reynolds number for all aspect ratios and all modes. As observed also by Vatistas et *al.* [1] for large aspect ratios, F is rather constant with Re but slightly increases with m.

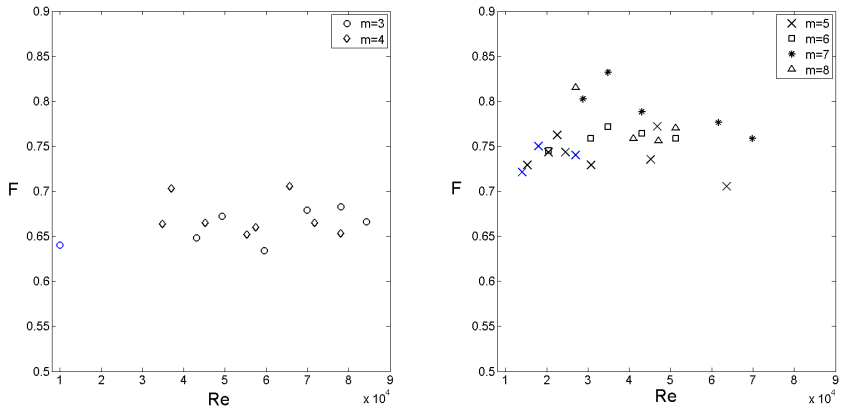

Figure 4: Dimensionless azimuthal velocity F of the polygon patterns deduced from the flow visualizations (black symbols) and the DNS (blue symbols) for $0.0143 \leq G \leq 0.143$.

Spiral patterns coexisting with a pentagonal structure have been observed experimentally and numerically (Fig.5). Figures 5b-d show that the spirals are characterized by a relatively high turbulence kinetic energy, and that they flow radially inward from the rotor to the free surface.The spirals move slower than the vortices at around 16.6% of the pentagon frequency. These are positive spiral patterns as they are rolled up in the same sense as the rotor. These spirals are very similar to the SRJ2 spirals of Poncet and Chauve [7] in a rotor-stator cavity with throughflow as they correspond also to a crossflow instability due to the inflexion point in the axial profile of the mean radial velocity. Their main characteristics are summed up in Table 1. Their inclination angle remains small compared to the values obtained by [7] ($\varepsilon \to 70°$). The number of spiral arms $28 \leq n \leq 40$ is also much lower: $n \to 90$ in [7]. A weak hysteresis is observed on the thresholds

of the spiral instability. $n = 29$ spiral arms with a positive angle $\varepsilon \simeq 25°$ have been observed numerically (Fig.5b-d), in excellent agreement with the experiment.

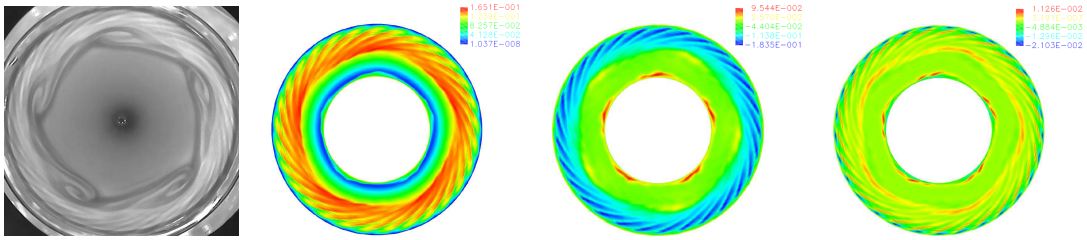

(a) (b) (c) (d)

Figure 5: Crossflow instability: (a) experimental results for $\eta = 0$, $Re = 24630$ (spin-up) and $G = 0.0714$; DNS results ($73\times192\times65$ mesh points in the (r, θ, z) directions with $\delta t = 5\times10^{-5}\Omega^{-1}$) for $\eta = 0.5$, $Re = 27000$ and $G = 0.0714$ at $z/e = 0.97$: (b) turbulence kinetic energy k^*, (c) instantaneous radial V_r^* and (d) axial V_z^* velocities.

G	Re (spin-up)	Re (spin-down)	n	ε (°)	r/R_o
0.0714	$24630 - 43102$	$16420 - 36945$	$28 - 30$	$23 - 25$	$0.85 - 0.89$
0.0429	$30788 - 57470$	$24630 - 45155$	$38 - 40$	$14 - 19$	$0.88 - 0.92$

Table 1: Characteristics of the spirals obtained experimentally.

4 Conclusion

One has reported a shear-layer instability developed on a rotating disk with a free surface as a sharp-cornered polygonal pattern with m vortices. The stability diagram has been established highlighting large hysteresis cycles. Modes up to $m = 8$ have been observed with a particular emphasis for the pentagonal structure. This pattern produced by the appearance of a secondary flow and the destabilization of the Stewartson layer along the casing rotates at 73.5% of the rotor speed. It may coexist with a crossflow instability appearing a positive spirals located along the shroud. Further DNS calculations are now required to understand the discrepancies between the experiments and the linear stability analysis of Kahouadji [4] for low aspect ratios $G \leq 0.06$.

References

[1] Vatistas, G.H., Ait Abderrahmane, H. & Siddiqui, M.H.K.: Experimental confirmation of Kelvin's equilibria. *Phys. Rev. Letters*, vol.100 (2008) 174503.

[2] Bergmann, R., Tophøj, L., Homan, T., Hersen, P., Andersen, A. & Bohr, T.: Polygon formation and surface flow on a rotating fluid surface. *J. Fluid Mech.*, vol.679 (2011) pp.415–431.

[3] Poncet, S. & Chauve, M.P.: Shear-layer instability in a rotating system. *J. Flow Visualization & Image Processing*, vol.14(1) (2007) pp.85–105.

[4] Kahouadji, L.: Analyse de stabilité linéaire découlements tournants en présence de surface libre. *Université Pierre et Marie Curie - Paris VI* (2011).

[5] Moisy, F., Doaré, O., Pasutto, T., Daube, O. & Rabaud, M.: Experimental and numerical study of the shear-layer instability between two-counter-rotating disks. *J. Fluid Mech.*, vol.507 (2004) pp.175–202.

[6] Niino, H. & Misawa, N.: An experimental and theoretical study of barotropic instability. *J. Atmos. Sci.*, vol.41 (1984) pp.1992–2011.

[7] Poncet, S. & Chauve, M.P.: Crossflow instability in a rotor-stator cavity with axial inward throughflow. *J. Fluid Mech.*, vol.545 (2005) pp.281–289.